Interface Stability of LiCl-rich Argyrodite Li_6PS_5Cl with Propylene Carbonate Boosts High-Performance Lithium Batteries

Yang Li,[a] William Arnold,[a] Jacek Jasinski,[a] Arjun Thapa,[a] Gamini Sumanasekera,[ac] Mahendra Sunkara,[ad] Badri Narayanan,[b] Thad Druffel,[a] Hui Wang[ab*]

[a]Conn Center for Renewable Energy Research, University of Louisville, 216 Eastern Parkway, Louisville 40292, KY, USA

[b]Department of Mechanical Engineering, University of Louisville, 332 Eastern Parkway, Louisville 40292, KY, USA

[c]Department of Physics & Astronomy, University of Louisville, 215 Eastern Parkway, Louisville 40208, KY, USA

[d]Department of Chemical Engineering, University of Louisville, 215 Eastern Parkway, Louisville 40292, KY, USA

*Corresponding Author: Hui Wang (hui.wang.1@louisville.edu)

Highlights:

1. LiCl-rich argyrodite SE ($Li_6PS_5Cl \cdot LiCl$) is synthesized by solvent-based method;
2. PC and excess LiCl in SE facilitates to form stable SEI layer at interface;
3. Improved interface stability significantly boosts battery cycling performance.

Abstract

In solid-state lithium (Li)-metal batteries (SSLMBs), sulfide-based Li-ion conductors represent one of the most popular solid electrolytes (SEs). However, the development of sulfide-based SSLMBs is significantly hampered by interfacial issues including large solid-solid contact resistance and serious side reactions at the SE/electrode interface. To address these issues, here, we demonstrated a simple and efficient strategy by using LiCl-rich argyrodite Li_6PS_5Cl (Li_6PS_5Cl·LiCl) SE and trace amount of propylene carbonate (PC) at the SE/electrode interface to facilitate the formation of stable and robust solid electrolyte interphase (SEI). The formed SEI not only serves as a buffer to passivate the interfacial reactions and suppress Li dendrite growth, but also acts as a bridge for Li-ion conduction to reduce the contact resistance. As a result, the Li‖Li symmetric cell exhibited long-term electrochemical cycling stability over 1000 h at a current density of 0.2 mA cm^{-2}. Furthermore, the assembled Li‖$Li_4Ti_5O_{12}$ (LTO) batteries delivered a specific capacity of 175 mAh g^{-1} at 0.2C, and remained an excellent specific capacity of 116 mAh g^{-1} after 200 cycles at a high current rate of 1C. These features indicate a feasible strategy to enhance the interfacial property of high-performance SSLMBs.

Key words: Li_6PS_5Cl, argyrodite electrolyte, LiCl-rich, interface, lithium battery

1. Introduction

Solid-state lithium (Li)-metal batteries (SSLMBs) are regarded as a promising candidate for next-generation energy storage due to the use of high-capacity Li metal anodes and solid electrolytes (SEs) with intrinsic safety [1−3]. Considering the flammability and the risk of leaking associated with liquid electrolytes (LEs), the replacement of LEs with nonflammable SEs provides an alternative solution to enhance the safety performance of batteries [4−7]. Over the past decades, significant research achievements have been made in exploring Li superionic conductors, such as perovskite-type [8], antiperovskite-type [9], thio-LISICON-type [10], NASICON-type [11,12], garnet [13] and sulfide glass/ceramic [14,15]. Among them, sulfide SEs usually offer higher conductivities (10^{-4}−10^{-2} S cm^{-1}) at room temperature [16−18], show favorable amenability for bulk fabrication due to cold-pressing induced densification [19,20]. In particular, lithium argyrodites Li_6PS_5X (X = Cl, Br, I), a representative family of sulfide SEs, have attracted strong research interests on their crystal structures [21], ion transport mechanisms [22,23,24] and battery cycling [25].

However, sulfide SEs generally suffer from serious instability issues towards metallic Li anode and oxide cathodes [26,27]. Significant interfacial reactions plus poor solid-solid contact at the sulfide SE/electrode interfaces result in high interfacial resistance, which is the major challenge for the development of sulfide-based SSLMBs [28,29]. Various attempts have been made to improve the interfacial stability in SSLMBs, including: (1) composite polymer electrolytes to improve the physical contact between electrolyte and electrode [30,31]; (2) an artificial buffer layer to

prevent interfacial reaction [32–34]; and (3) solid-liquid hybrid electrolyte at the interface to decrease the contact resistance [35,36]. Among these strategies, using a solid-liquid hybrid electrolyte is one of the most convenient approaches to improve the interfacial properties in SSLMBs [37,38]. However, this method requires to use expensive Li salt (e.g. LiTFSI, $LiPF_6$, $LiClO_4$) and extra additives (e.g. LiF, $LiNO_3$, etc.) to stabilize the interface. Replacing these high-priced Li salts with more economic alternatives would increase the affordability of the solid-state Li batteries.

Recent reports indicate that lithium halides (LiX, X = F, Cl, Br, I) can form a crystalline solid electrolyte interphase (SEI) film compatible with Li metal anode [29,39–41]. The formation of fluorine (F)-containing SEI from the dissolved Li salt in solvent has been demonstrated to efficiently stabilize the interface and suppress Li dendrite growth [29], but it requires the additional heat treatment to remove the solvent at interface. Instead, the incorporation of LiX into SEs is a more ideal solution, which not only enhances the ionic conductivity of sulfide SEs [42] but also improves the interface stability due to the presence of LiX in SEI [41,43]. In such halide doped sulfide SEs, the homogeneous distribution of LiX in bulk material is vital for the formation of a functional SEI at interface.

Herein, we demonstrate an efficient and economic strategy by using LiCl-rich argyrodite Li_6PS_5Cl SE (*in specific* $Li_6PS_5Cl{\cdot}LiCl$) and trace amount of PC to form stable and robust SEI at the SE/Li interface. A liquid-based synthesis method yields to $Li_6PS_5Cl{\cdot}LiCl$ SE with high crystallinity and homogeneous composition. The formed SEI layer not only bridges the SE/electrode interface for efficient Li-ion transport, but

also passivates the SE from Li metal for the side reactions with, thus suppressing Li dendrite growth (Scheme 1b). As a result, Li||Li symmetric cells shows long-term cycling stability up to 1000 h under 0.2 mA cm^{-2}. In addition, Li||Li_6PS_5Cl·LiCl/PC ||$Li_4Ti_5O_{12}$ (LTO) cells can deliver a high specific capacity of 175 mAh g^{-1} at 0.2 C and remain an impressive specific capacity of 116 mAh g^{-1} at 1C over 200 cycles. These features indicate a feasible approach to address interface instability issues to promote the development of high-performance Li metal batteries.

2. Experimental Section

2.1. Materials

Lithium sulfide (Li_2S) (99.9%, Alfa Aesar), phosphorus pentasulfide (P_2S_5) (98%, Acros Organics), lithium chloride (LiCl) (99%, Alfa Aesar), ethanol (99%, Merck), tetrahydrofuran (THF) (99%, VWR), propylene carbonate (PC) (99%, VWR), polyvinylidenedifluoride (PVDF) (99.9%, Sigma-Aldrich), N-methylpyrrolidone (NMP) (99.9%, Sigma-Aldrich) were used as purchased without further purification.

2.2. Synthesis of Li_6PS_5Cl·LiCl solid electrolyte

Li_6PS_5Cl·LiCl SE was synthesized through a solvent-based method *via* the stoichiometric reaction between Li_3PS_4, Li_2S and LiCl (mole ratio of 1:1:2) in ethanol medium, which is similar with our previous report [42, 44]. Briefly, Li_2S and LiCl were dissolved in ethanol, followed by adding β-Li_3PS_4 and stirring. Then, the mixture was heated at 90°C under vacuum until fully removal of ethanol, followed with heating treatment at 200°C for 1 hour. For comparison, Li_6PS_5Cl and

$Li_6PS_5Cl \cdot 2LiCl$ SEs were also synthesized following the stoichiometric ratio. For instance, the precursors of Li_3PS_4, Li_2S and LiCl (mole ratio of 1:1:3) yield to $Li_6PS_5Cl \cdot 2LiCl$ SE.

2.3. Characterizations

The morphology of the samples was examined using a TESCAN Vega3 scanning electron microscope (SEM). X-ray diffraction (XRD, Bruker D8 Discover) with nickel-filtered Cu Kα radiation (λ = 1.5418 Å) in the 2θ range of 10° to 70° was carried out for phase identification. X-ray photoelectron spectroscopy (XPS) spectra was recorded using Thermo VG Scientific ESCALAB XI X-ray photoelectron spectrometer microprobe.

For the electrochemical measurements, SE pellets were prepared by cold pressing the $Li_6PS_5Cl \cdot LiCl$ powder under ~400 MPa for around 1 min. The thickness of SE pellets is around 550–700 μm. Prior to electrochemical tests, various amount of PC was added on both sides of the $Li_6PS_5Cl \cdot LiCl$ SE pellet, denoted as PC-I (7.9 $\mu L/cm^2$), PC-II (11.8 $\mu L/cm^2$), and PC-III (15.8 $\mu L/cm^2$). The volume of the PC was quantified by a pipette with a metrological range from 0.5 μL to 20 μL. The prepared pellet was then sandwiched between two stainless steel plates to determine the ionic conductivity from room temperature to 90 °C. Electrochemical impedance spectroscopy (EIS) was measured by a Bio-Logic VSP300 electrochemical workstation in the frequency range from 0.1 to 5×10^6 Hz with an amplitude of 100 mV. The galvanostatic cycling test was conducted with symmetric cells using the

same electrochemical workstation at various current densities at room temperature. The electrochemical performance of the electrolyte was tested with $Li_4Ti_5O_{12}$ (LTO)‖Li cells. To prepare the electrode, LTO nanopowder, PVDF and Super P (80:10:10 in weight ratio) were mixed in N-methylpyrrolidone (NMP) to form a homogeneous slurry which was subsequently coated on aluminum foil. The prepared electrode with an active material loading of around 2.5 mg cm^{-2} was dried at 80 ºC under vacuum prior to use. Charge and discharge tests were performed over 1.0–3.0 V using 2032 coin cells after the cells were rested for 8 h.

3. Results and Discussion

Fig. 1a displays the XRD patterns of Li_6PS_5Cl·LiCl, whose characteristic diffraction peaks at 2θ=25.5, 30 and 31.2º are in good agreement with the (220), (311), and (222) planes in the argyrodite cubic structure (space group *F-43m*) [45,46]. Compared with Li_6PS_5Cl, the diffraction peaks detected at 34.9º and 49.9º are ascribed to the existence of LiCl. This indicates that the excess Cl cannot properly enter the Li_6PS_5Cl structure for solvent-based synthesis method that heat treated at 200 ºC. Instead, a heterogeneous composite of Li_6PS_5Cl·LiCl electrolyte is formed. The Arrhenius plot (Fig. 1b) shows that Li_6PS_5Cl·LiCl SE has an ionic conductivity of 3.0×10^{-4} S cm^{-1} at room temperature. This value is higher than that of Li_6PS_5Cl SE (2.0×10^{-4} S cm^{-1}) and Li_6PS_5Cl·2LiCl (6.5×10^{-5} S cm^{-1}) (Fig.S1), which is consistent with the previous report [42].

In this study, a trace amount of PC as the wetting agent was introduced at the SE/electrode interfaces to reduce the resistance for Li^+ transport in solid-state batteries. The effect of adding PC on the structure, morphology, and conductivity of Li_6PS_5Cl·LiCl SE was studied. In the XRD patterns of Li_6PS_5Cl·LiCl/PC sample (Fig. 1a), the main diffraction peaks of Li_6PS_5Cl·LiCl phase (2θ=25.5, 30 and 31.2°) are well maintained and there are no additional peaks, suggesting the structural stable of Li_6PS_5Cl·LiCl against PC. In addition, the chemical stability was examined by soaking Li_6PS_5Cl·LiCl pellet in PC solvent for 3 weeks. There is no visible color change and the pellet remains dense (Fig. S2), indicating that Li_6PS_5Cl·LiCl SE is chemically stable with PC. Regarding the ion transport, the Li_6PS_5Cl·LiCl/PC shows an ionic conductivity of 4.5×10^{-4} S cm^{-1} at room temperature, which is slightly higher than that of Li_6PS_5Cl·LiCl (3.0×10^{-4} S cm^{-1}) and Li_6PS_5Cl/PC (3.3×10^{-4} S cm^{-1}). The electrochemical impedance spectra (EIS) of Li_6PS_5Cl·LiCl and Li_6PS_5Cl·LiCl/PC SEs at various temperatures were shown in Fig. S3. As temperature increases, the impedance decreases and the steep linear spike at low frequency indicates the behavior of a typical ionic conductor

The morphologies of Li_6PS_5Cl·LiCl pellet and Li_6PS_5Cl·LiCl/PC pellet were characterized by scanning electron microscope (SEM). Li_6PS_5Cl·LiCl pellet shows a dense and smooth surface (Fig. 2a and 2b). In contrast, the surface of the Li_6PS_5Cl·LiCl/PC pellet becomes slightly rough due to the wettability of PC on the pellet surface (Fig. 2c and 2d). The elemental mapping images of cross-section (Fig. 2e) by energy dispersive spectroscopy (EDS) demonstrates the uniform distribution of

phosphorous (P), sulfur (S) and chloride (Cl), which indicates that adding PC only influence the surface and the majority of Li_6PS_5Cl·LiCl remain unchanged.

Fig. 3a presents the plating/stripping profiles of Li||Li symmetric cells with Li_6PS_5Cl·LiCl and Li_6PS_5Cl·LiCl/PC SEs from galvanostatic cycling tests, where the cells were periodically charged and discharged under 0.2 mA cm^{-2}. For the symmetric cell with Li_6PS_5Cl·LiCl SE, an obvious sharp drop in voltage can be observed after only 20 h cycling, indicating an internal short circuit due to the growth of Li dendrites [47,48]. This observation is consistent with previous reports which indicate that sulfide SEs suffer from low critical current density (CCD), where dendrite formation abruptly occurs in sulfide SEs even at a low current density [49,50]. This cell's impedance after cycling confirms a typical short circuit by dendrite formation (Fig. 3c). In contrast, the Li|| Li_6PS_5Cl·LiCl/PC||Li symmetric cell exhibited much better performance with stable cycling of up to 1000 h. It can be supported by the EIS measurements of the cell with Li_6PS_5Cl·LiCl/PC before and after cycling (Fig. 3b), where shows a slight increase in the impedance (500 to 600 Ω) due to the inevitable interface reaction. The SEM images of Li metal and SE in the Li||Li symmetric cells after cycling are shown in Fig. S4a–S4f). For the cell with bare Li_6PS_5Cl·LiCl SE, the morphological images of the Li metal and Li_6PS_5Cl·LiCl pellet after cycling are not uniform, and massive irregular Li dendrites are observed (Fig. S4a and S4b). However, for the cell with Li_6PS_5Cl·LiCl/PC after cycling, the surfaces remained uniform and smooth without Li dendrites formation (Fig. S4d and S4e). From the cross-sectional images (Fig. S4c and S3f), both SE pellets remained dense after

cycling. In addition, the Li‖Li_6PS_5Cl·LiCl/PC‖Li symmetric cell was cycled at various current densities of 0.1, 0.2, 0.5, 0.8 and 1.0 mA cm^{-2}, respectively (Fig. 3d). The voltage profiles increase with increasing current density due to the polarization effect. When the current density increases to 1.0 mA cm^{-2}, the voltage hysteresis remains stable without obvious polarization amplification, suggesting good cycling stability even at high current density [51,52].

To evaluate the effect of PC amount on the electrochemical performance, LTO‖ Li_6PS_5Cl·LiCl/PC‖Li cells with different amounts of PC at interface were assembled and denoted as Li_6PS_5Cl·LiCl/PC-I (7.9 μL/cm^2), Li_6PS_5Cl·LiCl/PC-II (11.8 μL/cm^2), and Li_6PS_5Cl·LiCl/PC-III (15.8 μL/cm^2), respectively. It was found that the total resistance of the cell with Li_6PS_5Cl·LiCl SE was dramatically reduced after adding PC at interface. As evidenced in Fig. S5, the resistance of the cell decreases from 8000 Ω for the cell with bare Li_6PS_5Cl·LiCl SE to 1900 Ω for the Li_6PS_5Cl·LiCl/PC-I (7.9 μL/cm^2), continues to drop to 420 Ω for the cell with Li_6PS_5Cl·LiCl/PC-III (15.8 μL/cm^2). The presence of PC at interface plays a critical role in decreasing the interfacial resistance, which is mainly ascribed to efficient ion transport due to the penetration of PC into the cathode. The remarkably decreased resistance at SE/electrode interface is beneficial for the improvement of electrochemical property.

Fig. 4a displays the cycling performance of LTO‖Li cells with Li_6PS_5Cl·LiCl/PC at 0.2 C compared to the cells with Li_7PS_6/PC and Li_6PS_5Cl/PC. Among three SEs, the cell with Li_6PS_5Cl·LiCl/PC exhibits a high specific capacity (175 mAh g^{-1}), indicating a favorable interface and a positive effect of LiCl on the enhancement of

electrochemical properties. Fig. S6 displays the initial charge/discharge curves of LTO‖ Li_6PS_5Cl·LiCl ‖Li cells without and with PC at interface. In the former case, the cell with bare SE without modified electrode surfaces showed irregular charge/discharge curves and exhibited very low capacity due to huge interface resistance [32,33,53]. On the other hand, the cycling performance of the LTO‖ Li_6PS_5Cl·LiCl/PC‖Li cells with various amount of PC at the interface was compared at 0.2 C (Fig. 4b). By using Li_6PS_5Cl·LiCl/PC-I (7.9 μL/cm^2), the cell delivers a specific capacity of 168 mAh g^{-1} but only a coulombic efficiency of 47%. Such a low coulombic efficiency is attributed to the fact that the amount of PC-I is too small to completely wet the interface. When the amount increases to PC-III (15.8 μL/cm^2), the LTO‖Li cell achieves an initial specific capacity of 175 mAh g^{-1} and a coulombic efficiency of 88% (Fig. S6b). The LTO‖ Li_6PS_5Cl·LiCl/PC-III‖Li cell exhibited the highest specific capacity and best cycling stability. After cycling, the impedance of the cell slightly increased due to the SEI layer formation at the interface (Fig. S7). In addition, when the C-rate increased to 1C, the LTO‖ Li_6PS_5Cl·LiCl/PC-III‖Li cell delivered stable cycling capability maintained an impressive specific capacity of 116 mAh g^{-1} over 200 cycles with a coulombic efficiency of ~99.9% (Fig. 4c). Fig. S8 shows the discharge/charge curves of the cell under the current rate of 1C at the 1^{st}, 50^{th}, 100^{th} and 200^{th} cycles, all of which display typical discharge/charge plateaus of the LTO‖Li cell at around 1.55 V.

In addition, the rate capability of the LTO‖Li_6PS_5Cl·LiCl/PC-III‖Li cell was investigated at various current rates of 0.2 C, 0.5 C, 1 C and 2 C. Fig. 4d shows that

the discharge capacity decreases as increasing current rate due to the polarization effect. This cell delivers a decent capacity of 80 mAh g^{-1} even at a high current rate of 2C. The cell also exhibits an ability to recover its capacity when the current rate changed from 2 C to 0.2 C after 20 discharge/charge cycles. The voltage profiles of the cell cycled at various current rates are presented in Fig. 4e. For the LTO||Li_6PS_5Cl·LiCl/PC-III||Li cell, such excellent electrochemical performance is attributed to the stable SEI at SE/electrode interfaces owing to the presence of excess LiCl in the SE as well as the PC as a wetting agent.

To analyze the interfacial properties between the electrolyte and Li metal, the LTO||Li_6PS_5Cl·LiCl/PC-III||Li cell after cycling was disassembled and the surface of the SE was inspected by SEM and XPS. Fig. S9 shows the surface morphology of Li_6PS_5Cl·LiCl SE recovered from the cycled LTO||Li_6PS_5Cl·LiCl/PC-III||Li cell. After prolonged cycling, a smooth and dense surface of SE was observed. The detailed XPS spectra fitting of S 2p, P 2p, Cl 2p, C 1s and O 1s were analyzed to further identify the chemical properties of the SEI at interface. It is known that the interfacial reactions between bare sulfide SEs (i.e. $Li_{10}GeP_2S_{12}$) and Li metal yield to the products of Li_2S, Li_3P as well as reduced phosphorus species [54–56]. However, the cycled LTO||Li_6PS_5Cl·LiCl/PC-III||Li cell has a totally different case. As shown in Fig. 5 and Fig. S10, the high-resolution spectra of S 2p, Cl 2p and P 2p exhibit no change after cycling, indicating the decomposition/reduction reaction between sulfide SE and Li metal was prevented by the SEI formation. The spectra of C 1s shows a clear new peak at around 290.2 eV, corresponding to the detected CO_3^{2-} from the

Li_2CO_3 due to the reaction between PC and Li metal, which can be further confirmed by the spectra of O 1s [36,57,58]. These results indicate that an interfacial SEI film composed of Li salt (LiCl) and organic compounds is formed between sulfide SE and Li metal after electrochemical cycling.

4. Conclusions

In summary, we demonstrated an effective and feasible strategy to address the interfacial issues in sulfide-based lithium batteries by using LiCl-rich argyrodite SE (Li_6PS_5Cl·LiCl) and PC as wetting agent. The Li_6PS_5Cl·LiCl SE coupled with trace amount PC could facilitate to form stable SEI to prevent the interfacial reactions between SE and Li metal. As a result, Li‖Li symmetric cells with stable electrochemical cycling over 1000 h at a current density of 0.2 mA cm^{-2} have been achieved. In addition, LTO‖ Li_6PS_5Cl·LiCl/PC-III‖Li cells delivered a high specific capacity of 175 mAh g^{-1} at 0.2 C, and remained an impressive specific capacity of 116 mAh g^{-1} at 1 C over 200 cycles. These features indicate that the developed approach provides an alternative strategy to enhance the interfacial property of high-performance lithium batteries.

Conflicts of Interest

The authors declare no competing financial conflicts.

Acknowledgments

The authors thank the support from U.S. Department of Energy's Office of Energy Efficiency and Renewable Energy (EERE) Grant under the Vehicle Technologies Office (award No. EE0008866), Conn Center for Renewable Energy Research, and the EVPI Internal Grant of the University of Louisville. W.A. thanks the support from the NASA KY Graduate Fellowship (award number NNX15AR69H).

References

[1] A. Manthiram, X. Yu, S. Wang, Lithium battery chemistries enabled by solid-state electrolytes, Nat. Rev. Mater., 2 (2017), 16103.

[2] Z. Gao, H. Sun, L. Fu, F. Ye, Y. Zhang, W. Luo, Y. Huang, Promises, challenges, and recent progress of inorganic solid-state electrolytes for all-solid-state lithium batteries, Adv. Mater., 30 (2018), 1705702.

[3] D. Lin, Y. Liu, Y. Cui, Reviving the lithium metal anode for high-energy batteries, Nat. Nanotechnol., 12 (2017), 194.

[4] X.-B. Cheng, C.-Z. Zhao, Y.-X. Yao, H. Liu, Q. Zhang, Recent advances in energy chemistry between solid-state electrolyte and safe lithium-metal anodes, Chem, 5 (2019), 74–79.

[5] J. Janek, W.G. Zeier, A solid future for battery development, Energy, 500 (2016), 300.

[6] J. Lau, R.H. DeBlock, D.M. Butts, D.S. Ashby, C.S. Choi, B.S. Dunn, Sulfide solid electrolytes for lithium battery applications, Adv. Energy Mater., 8 (2018), 1800933.

[7] L. Fan, S. Wei, S. Li, Q. Li, Y. Lu, Recent progress of the solid-state electrolytes for high-energy metal-based batteries, Adv. Energy Mater., 8 (2018), 1702657.

[8] J.F. Ihlefeld, P.G. Clem, B.L. Doyle, P.G. Kotula, K.R. Fenton, C.A. Apblett, Fast lithium-ion conducting thin-film electrolytes integrated directly on flexible substrates for high-power solid-state batteries, Adv. Mater., 23 (2011), 5663–5667.

[9] X. Lü, J.W. Howard, A. Chen, J. Zhu, S. Li, G. Wu, P. Dowden, H. Xu, Y. Zhao, Q. Jia, Antiperovskite Li_3OCl superionic conductor films for solid-state Li-ion batteries, Adv. Sci., 3 (2016), 1500359.

[10] S. Muy, J.C. Bachman, L. Giordano, H.-H. Chang, D.L. Abernathy, D. Bansal, O. Delaire, S. Hori, R. Kanno, F. Maglia, Tuning mobility and stability of lithium ion conductors based on lattice dynamics, Energy Environ. Sci., 11 (2018), 850–859.

[11] Y. Noda, K. Nakano, H. Takeda, M. Kotobuki, L. Lu, M. Nakayama, Computational and experimental investigation of the electrochemical stability and Li-ion conduction mechanism of $LiZr_2(PO_4)_3$, Chem. Mater., 29 (2017), 8983–8991.

[12] R. DeWees, H. Wang, Synthesis and properties of NASICON-type LATP and LAGP solid electrolytes, ChemSusChem, 12 (2019), 7313–7325.

[13] L. Buannic, B. Orayech, J.-M. Lopez Del Amo, J. Carrasco, N.A. Katcho, F.d.r. Aguesse, W. Manalastas, W. Zhang, J. Kilner, A. Llordés, Dual substitution strategy to enhance Li^+ ionic conductivity in $Li_7La_3Zr_2O_{12}$ solid electrolyte, Chem. Mater., 29 (2017), 1769–1778.

[14] D.Y. Oh, Y.J. Nam, K.H. Park, S.H. Jung, S.J. Cho, Y.K. Kim, Y.G. Lee, S.Y. Lee, Y.S. Jung, Excellent compatibility of solvate ionic liquids with sulfide solid

electrolytes: toward favorable ionic contacts in bulk-type all-solid-state lithium-ion batteries, Adv. Energy Mater., 5 (2015), 1500865.

[15] Y. Kato, S. Hori, T. Saito, K. Suzuki, M. Hirayama, A. Mitsui, M. Yonemura, H. Iba, R. Kanno, High-power all-solid-state batteries using sulfide superionic conductors, Nat. Energy, 1 (2016), 16030.

[16] Z. Zhang, Y. Shao, B. Lotsch, Y.-S. Hu, H. Li, J. Janek, L.F. Nazar, C.-W. Nan, J. Maier, M. Armand, New horizons for inorganic solid state ion conductors, Energy Environ. Sci., 11 (2018), 1945−1976.

[17] Q. Zhang, D. Cao, Y. Ma, A. Natan, P. Aurora, H. Zhu, Sulfide-based solid-state electrolytes: synthesis, stability, and potential for all-solid-state batteries, Adv. Mater., 31 (2019), 1901131.

[18] S. Chen, D. Xie, G. Liu, J.P. Mwizerwa, Q. Zhang, Y. Zhao, X. Xu, X. Yao, Sulfide solid electrolytes for all-solid-state lithium batteries: structure, conductivity, stability and application, Energy Storage Mater., 14 (2018), 58−74.

[19] A. Hayashi, K. Noi, A. Sakuda, M. Tatsumisago, Superionic glass-ceramic electrolytes for room-temperature rechargeable sodium batteries, Nat. Commun., 3 (2012), 856.

[20] R. Kanno, M. Murayama, Lithium ionic conductor thio-LISICON: the Li_2S-GeS_2-P_2S_5 system, J. Electrochem. Soc., 148 (2001), A742−A746.

[21] H. J. Deiseroth, S. T. Kong, H. Eckert, J. Vannahme, C. Reiner, T. Zaiß, M. Schlosser, Li_6PS_5X: a class of crystalline Li-rich solids with an unusually high Li^+ mobility, Angew. Chem., 120 (2008), 767−770.

[22] C. Yu, S. Ganapathy, N. J. de Klerk, I. Roslon, E. R. van Eck, A. P. Kentgens, M. Wagemaker, Unravelling Li-ion transport from picoseconds to seconds: bulk versus interfaces in an argyrodite Li_6PS_5Cl-Li_2S all-solid-state Li-ion battery, J. Am. Chem. Soc., 138 (2016), 11192−11201.

[23] M. A. Kraft, S. P. Culver, M. Calderon, F. Böcher, T. Krauskopf, A. Senyshyn, C. Dietrich, A. Zevalkink, J. Janek, W. G. Zeier, Influence of lattice polarizability on the ionic conductivity in the lithium superionic argyrodites Li_6PS_5X (X = Cl, Br, I), J. Am. Chem. Soc., 139 (2017), 10909−10918.

[24] P. R. Rayavarapu, N. Sharma, V. K. Peterson, S. Adams, Variation in structure and Li^+-ion migration in argyrodite-type Li_6PS_5X (X = Cl, Br, I) solid electrolytes, J. Solid State Electrochem., 16 (2012), 1807−1813.

[25] C. Yu, S. Ganapathy, E. R. Van Eck, H. Wang, S. Basak, Z. Li, M. Wagemaker, Accessing the bottleneck in all-solid state batteries, lithium-ion transport over the solid-electrolyte-electrode interface, Nat. Commun., 8 (2017), 1−9.

[26] T. K. Schwietert, V. A. Arszelewska, C. Wang, C. Yu, A. Vasileiadis, N. J. de Klerk, J. Hageman, T. Hupfer, I. Kerkamm, Y. Xu, E. van der Maas, E. M. Kelder, S. Ganapathy, M. Wagemaker, Clarifying the relationship between redox activity and electrochemical stability in solid electrolytes, Nat. Mater., 19 (2020), 428−435.

[27] C. Yu, Y. Li, W. Li, K. R. Adair, F. Zhao, M. Willans, L. Liang, Y. Zhao, C. Wang, S. Deng, R. Li, H. Huang, S. Lu, T. K. Sham, Y. Huang, X. Sun, Enabling ultrafast ionic conductivity in Br-based lithium argyrodite electrolytes for solid-state batteries with different anodes, Energy Stor. Mater., 30 (2020), 238−249.

[28] Z. Zhang, S. Chen, J. Yang, J. Wang, L. Yao, X. Yao, P. Cui, X. Xu, Interface re-engineering of $Li_{10}GeP_2S_{12}$ electrolyte and lithium anode for all-solid-state lithium batteries with ultralong cycle life, ACS Appl. Mater. Interfaces, 10 (2018), 2556−2565.

[29] R. Xu, F. Han, X. Ji, X. Fan, J. Tu, C. Wang, Interface engineering of sulfide electrolytes for all-solid-state lithium batteries, Nano Energy, 53 (2018), 958−966.

[30] Y. Zhao, C. Wu, G. Peng, X. Chen, X. Yao, Y. Bai, F. Wu, S. Chen, X. Xu, A new solid polymer electrolyte incorporating $Li_{10}GeP_2S_{12}$ into a polyethylene oxide matrix for all-solid-state lithium batteries, J. Power Sources, 301 (2016), 47−53.

[31] J. Zhang, C. Zheng, J. Lou, Y. Xia, C. Liang, H. Huang, Y. Gan, X. Tao, W. Zhang, Poly(ethylene oxide) reinforced Li_6PS_5Cl composite solid electrolyte for all-solid-state lithium battery: Enhanced electrochemical performance, mechanical property and interfacial stability, J. Power Sources, 412 (2019), 78−85.

[32] X. Fan, X. Ji, F. Han, J. Yue, J. Chen, L. Chen, T. Deng, J. Jiang, C. Wang, Fluorinated solid electrolyte interphase enables highly reversible solid-state Li metal battery, Sci. Adv., 4 (2018), 9245.

[33] C. Wang, K.R. Adair, J. Liang, X. Li, Y. Sun, X. Li, J. Wang, Q. Sun, F. Zhao, X. Lin, R. Li, H, Huang, L. Zhang, R. Yang, S. Lu, X. Sun, Solid-state plastic crystal electrolytes: effective protection interlayers for sulfide-based all-solid-state lithium metal batteries, Adv. Funct. Mater., 29 (2019), 1900392.

[34] S.-S. Chi, Y. Liu, N. Zhao, X. Guo, C.-W. Nan, L.-Z. Fan, Solid polymer electrolyte soft interface layer with 3D lithium anode for all-solid-state lithium

batteries, Energy Storage Mater., 17 (2019), 309−316.

[35] B. Xu, H. Duan, H. Liu, C.A. Wang, S. Zhong, Stabilization of garnet/liquid electrolyte interface using superbase additives for hybrid Li batteries, ACS Appl. Mater. Interfaces, 9 (2017), 21077−21082.

[36] C. Wang, Q. Sun, Y. Liu, Y. Zhao, X. Li, X. Lin, M.N. Banis, M. Li, W. Li, K.R. Adair, D. Wang, J. Liang, R. Li, L. Zhang, R. Yang, S. Lu, X. Sun, Boosting the performance of lithium batteries with solid-liquid hybrid electrolytes: interfacial properties and effects of liquid electrolytes, Nano Energy, 48 (2018), 35−43.

[37] J. Liang, J. Luo, Q. Sun, X. Yang, R. Li, X. Sun, Recent progress on solid-state hybrid electrolytes for solid-state lithium batteries, Energy Storage Mater., 21 (2019), 308−334.

[38] M. Keller, A. Varzi, S. Passerini, Hybrid electrolytes for lithium metal batteries, J. Power Sources, 392 (2018), 206−225.

[39] Y. Lu, Z. Tu, L.A. Archer, Stable lithium electrodeposition in liquid and nanoporous solid electrolytes, Nat. Mater., 13 (2014), 961.

[40] L. Lin, F. Liang, K. Zhang, H. Mao, J. Yang, Y. Qian, Lithium phosphide/lithium chloride coating on lithium for advanced lithium metal anode, J. Mater. Chem. A, 6 (2018), 15859−15867.

[41] F. Han, J. Yue, X. Zhu, C. Wang, Suppressing Li dendrite formation in Li_2S-P_2S_5 solid electrolyte by LiI incorporation, Adv. Energy Mater., 8 (2018), 1703644.

[42] W. Arnold, D. A. Buchberger, Y. Li, M. Sunkara, T. Druffel, H. Wang, Halide doping effect on solvent-synthesized lithium argyrodites Li_6PS_5X (X= Cl, Br, I) superionic conductors, J. Power Sources, 464 (2020), 228158.

[43] E. Rangasamy, Z. Liu, M. Gobet, K. Pilar, G. Sahu, W. Zhou, H. Wu, S. Greenbaum, C. Liang, An iodide-based $Li_7P_2S_8I$ superionic conductor, J. Am. Chem. Soc., 137 (2015), 1384−1387.

[44] D.A. Ziolkowska, W. Arnold, T. Druffel, M. Sunkara, H. Wang, Rapid and economic synthesis of a Li_7PS_6 solid electrolyte from a liquid approach, ACS Appl. Mater. Interfaces, 11 (2019), 6015−6021.

[45] C. Yu, L. van Eijck, S. Ganapathy, M. Wagemaker, Synthesis, structure and electrochemical performance of the argyrodite Li_6PS_5Cl solid electrolyte for Li-ion solid state batteries, Electrochim. Acta, 215 (2016), 93−99.

[46] C. Yu, S. Ganapathy, J. Hageman, L. van Eijck, E.R. van Eck, L. Zhang, T. Schwietert, S. Basak, E.M. Kelder, M. Wagemaker, Facile synthesis toward the optimal structure-conductivity characteristics of the argyrodite Li_6PS_5Cl solid-state electrolyte, ACS Appl. Mater. Interfaces, 10 (2018), 33296−33306.

[47] J. Zhang, Y. Bai, X.-G. Sun, Y. Li, B. Guo, J. Chen, G.M. Veith, D.K. Hensley, M.P. Paranthaman, J.B. Goodenough, Superior conductive solid-like electrolytes: nanoconfining liquids within the hollow structures, Nano Lett., 15 (2015), 3398−3402.

[48] Y. Lu, K. Korf, Y. Kambe, Z. Tu, L.A. Archer, Ionic-liquid-nanoparticle hybrid electrolytes: applications in lithium metal batteries, Angew. Chem. Int. Ed., 53 (2014),

488−492.

[49] L. Porz, T. Swamy, B.W. Sheldon, D. Rettenwander, T. Frömling, H.L. Thaman, S. Berendts, R. Uecker, W.C. Carter, Y.M. Chiang, Mechanism of lithium metal penetration through inorganic solid electrolytes, Adv. Energy Mater., 7 (2017), 1701003.

[50] E.J. Cheng, A. Sharafi, J. Sakamoto, Intergranular Li metal propagation through polycrystalline $Li_{6.25}Al_{0.25}La_3Zr_2O_{12}$ ceramic electrolyte, Electrochim. Acta, 223 (2017), 85−91.

[51] Z. Wan, D. Lei, W. Yang, C. Liu, K. Shi, X. Hao, L. Shen, W. Lv, B. Li, Q.H. Yang, Low resistance-integrated all-solid-state battery achieved by $Li_7La_3Zr_2O_{12}$ nanowire upgrading polyethylene oxide (PEO) composite electrolyte and PEO cathode binder, Adv. Funct. Mater., 29 (2019), 1805301.

[52] H. Chen, A. Pei, D. Lin, J. Xie, A. Yang, J. Xu, K. Lin, J. Wang, H. Wang, F. Shi, D. Boyle, Y. Cui, Uniform high ionic conducting lithium sulfide protection layer for stable lithium metal anode, Adv. Energy Mater., 9 (2019), 1900858.

[53] D.H. Kim, D.Y. Oh, K.H. Park, Y.E. Choi, Y.J. Nam, H.A. Lee, S.-M. Lee, Y.S. Jung, Infiltration of solution-processable solid electrolytes into conventional Li-ion-battery electrodes for all-solid-state Li-ion batteries, Nano Lett., 17 (2017), 3013−3020.

[54] J. Auvergniot, A. Cassel, D. Foix, V. Viallet, V. Seznec, R. Dedryvère, Redox activity of argyrodite Li_6PS_5Cl electrolyte in all-solid-state Li-ion battery: an XPS study, Solid State Ion., 300 (2017), 78−85.

[55] S. Wenzel, S.J. Sedlmaier, C. Dietrich, W.G. Zeier, J. Janek, Interfacial reactivity and interphase growth of argyrodite solid electrolytes at lithium metal electrodes, Solid State Ion., 318 (2018), 102−112.

[56] S. Wenzel, S. Randau, T. Leichtweiß, D.A. Weber, J. Sann, W.G. Zeier, J.r. Janek, Direct observation of the interfacial instability of the fast ionic conductor $Li_{10}GeP_2S_{12}$ at the lithium metal anode, Chem. Mater., 28 (2016), 2400−2407.

[57] S. Dalavi, P. Guduru, B.L. Lucht, Performance enhancing electrolyte additives for lithium ion batteries with silicon anodes, J. Electrochem. Soc., 159 (2012), A642−A646.

[58] Y. Gao, R. Yi, Y.C. Li, J. Song, S. Chen, Q. Huang, T.E. Mallouk, D. Wang, General method of manipulating formation, composition, and morphology of solid-electrolyte interphases for stable Li-alloy anodes, J. Am. Chem. Soc., 139 (2017), 17359−17367.

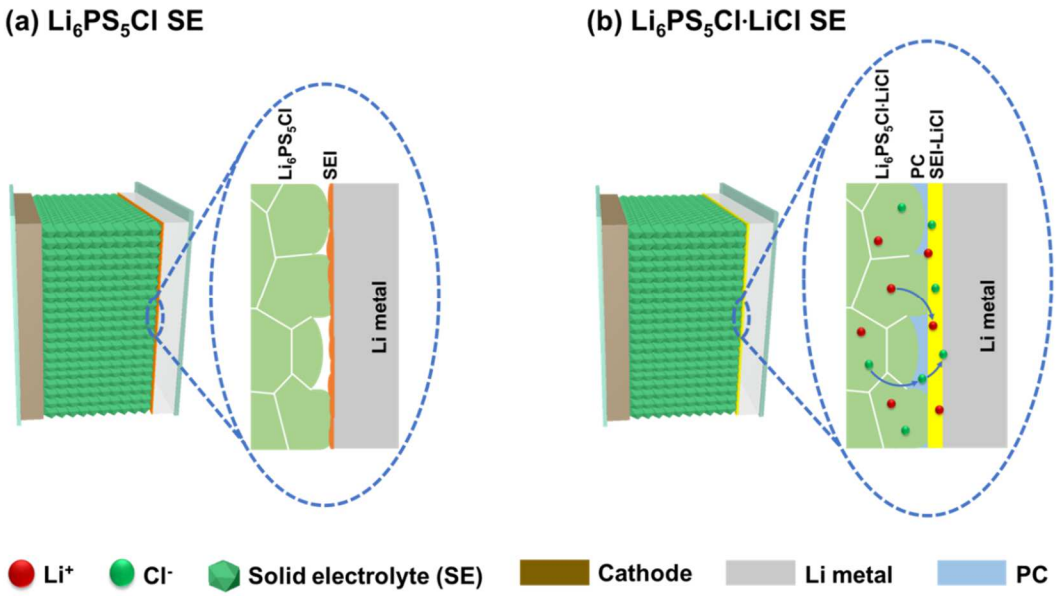

Scheme 1. Schematic diagram of batteries with (a) bare Li_6PS_5Cl SE, and (b) Li_6PS_5Cl·LiCl SE with PC at interface.

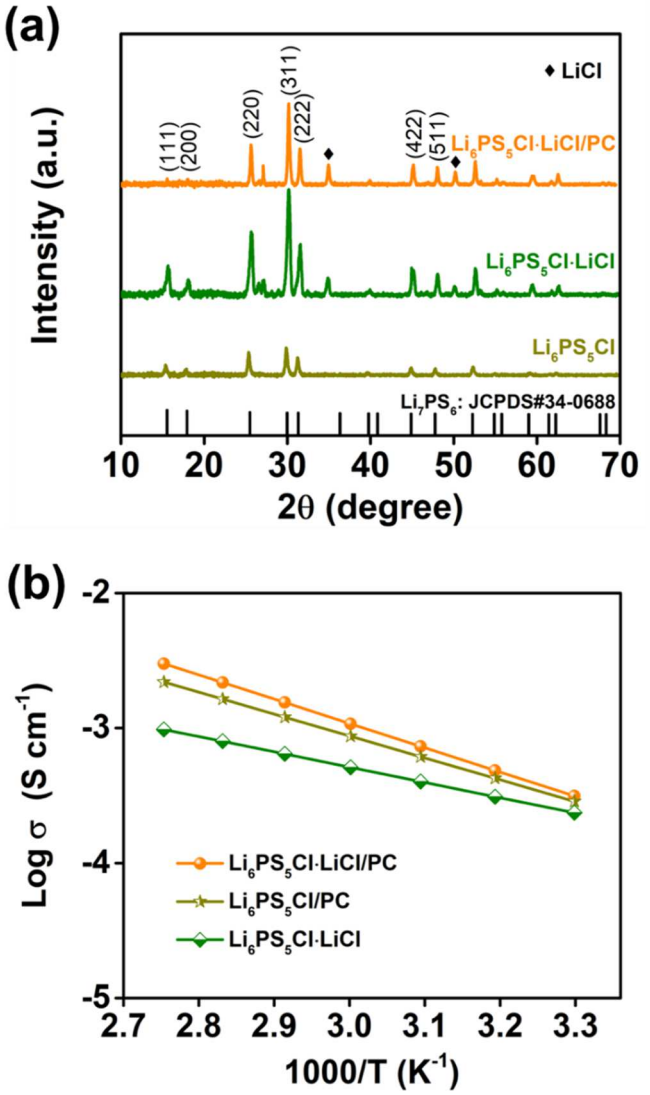

Fig. 1. (a) XRD patterns of Li_6PS_5Cl, $Li_6PS_5Cl{\cdot}LiCl$ and $Li_6PS_5Cl{\cdot}LiCl/PC$. (b) Arrhenius plots of $Li_6PS_5Cl{\cdot}LiCl$, Li_6PS_5Cl/PC and $Li_6PS_5Cl{\cdot}LiCl/PC$ SEs.

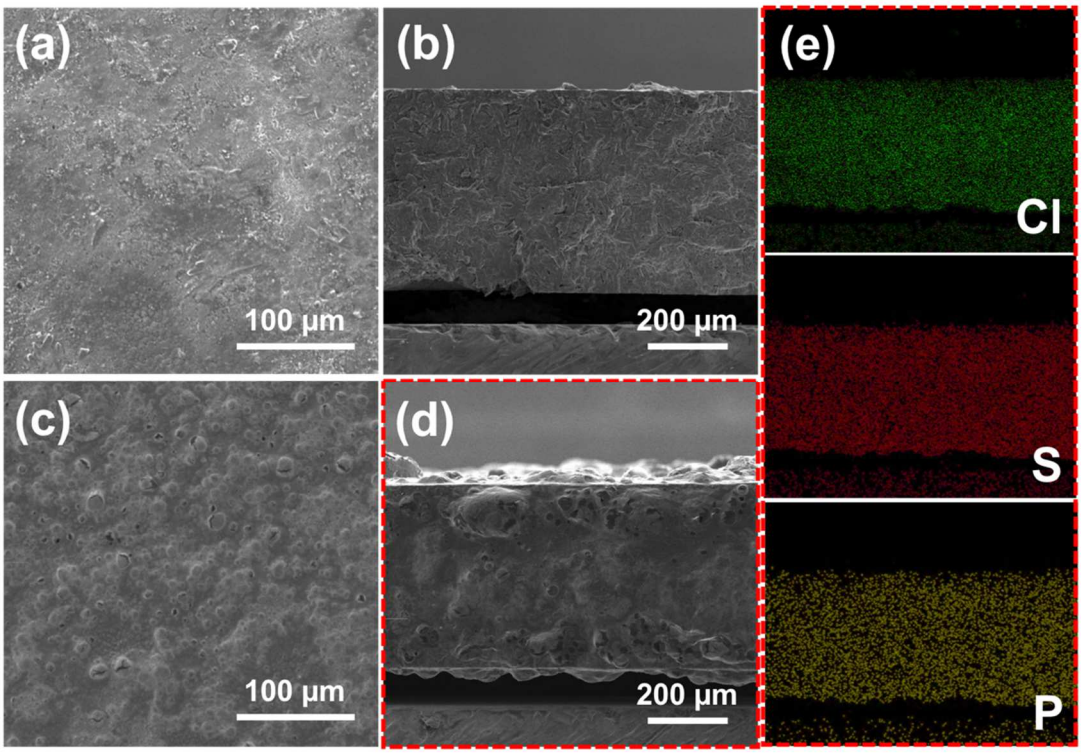

Fig. 2. SEM images of top surface and cross-section for Li_6PS_5Cl·LiCl SE (a,b) and Li_6PS_5Cl·LiCl with PC (c,d). (e) EDS mappings of P, S and Cl distributions for the Li_6PS_5Cl·LiCl/PC pellet.

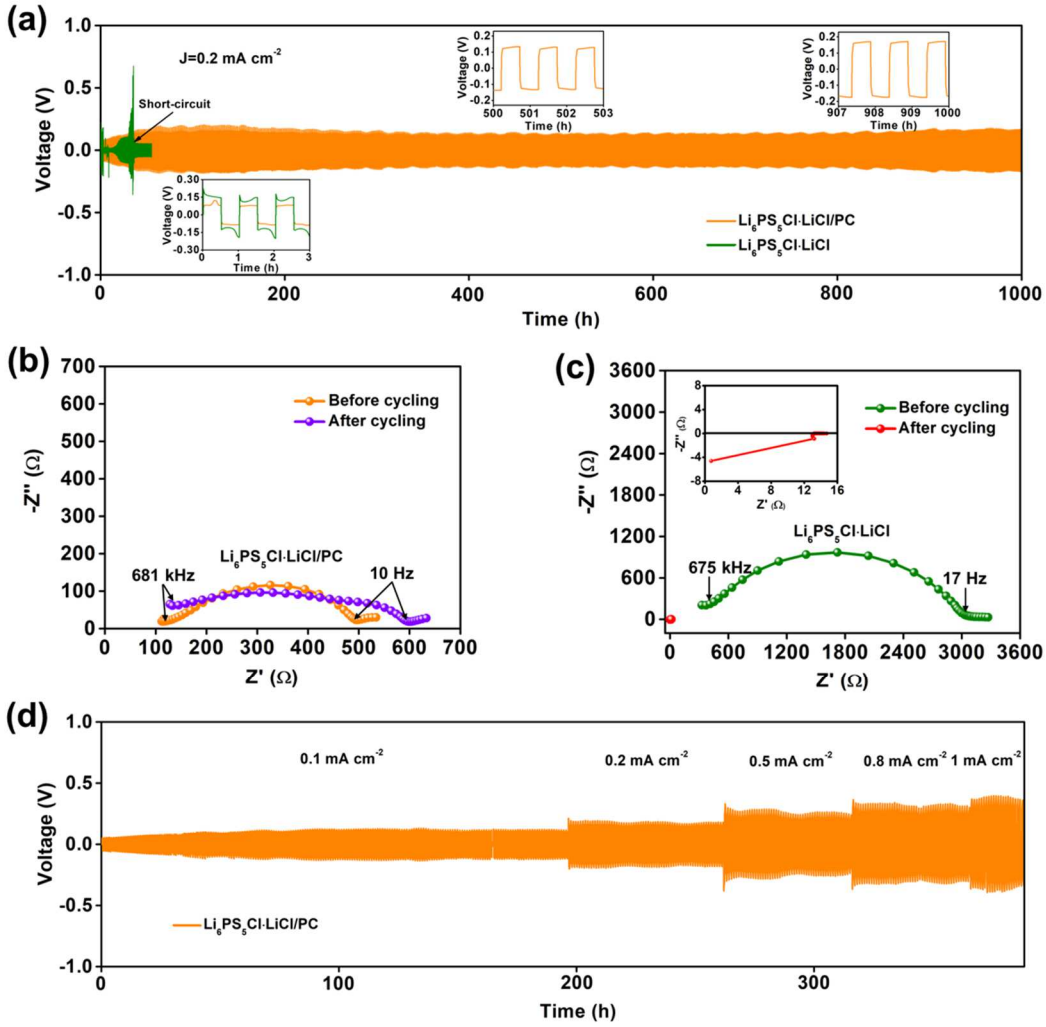

Fig. 3. (a) Voltage profiles of Li symmetric cells with Li_6PS_5Cl·LiCl without and with PC at interface at current density of 0.2 mA cm^{-2} (the areal capacity of 0.1 mAh cm^{-2}). EIS spectra of Li||Li symmetric cells with (b) Li_6PS_5Cl·LiCl with PC and (c) Li_6PS_5Cl·LiCl SE without PC before and after cycling. (d) Voltage profiles of Li symmetric cell with Li_6PS_5Cl·LiCl/PC cycled at various current densities of 0.1, 0.2, 0.5, 0.8 and 1.0 mA cm^{-2}.

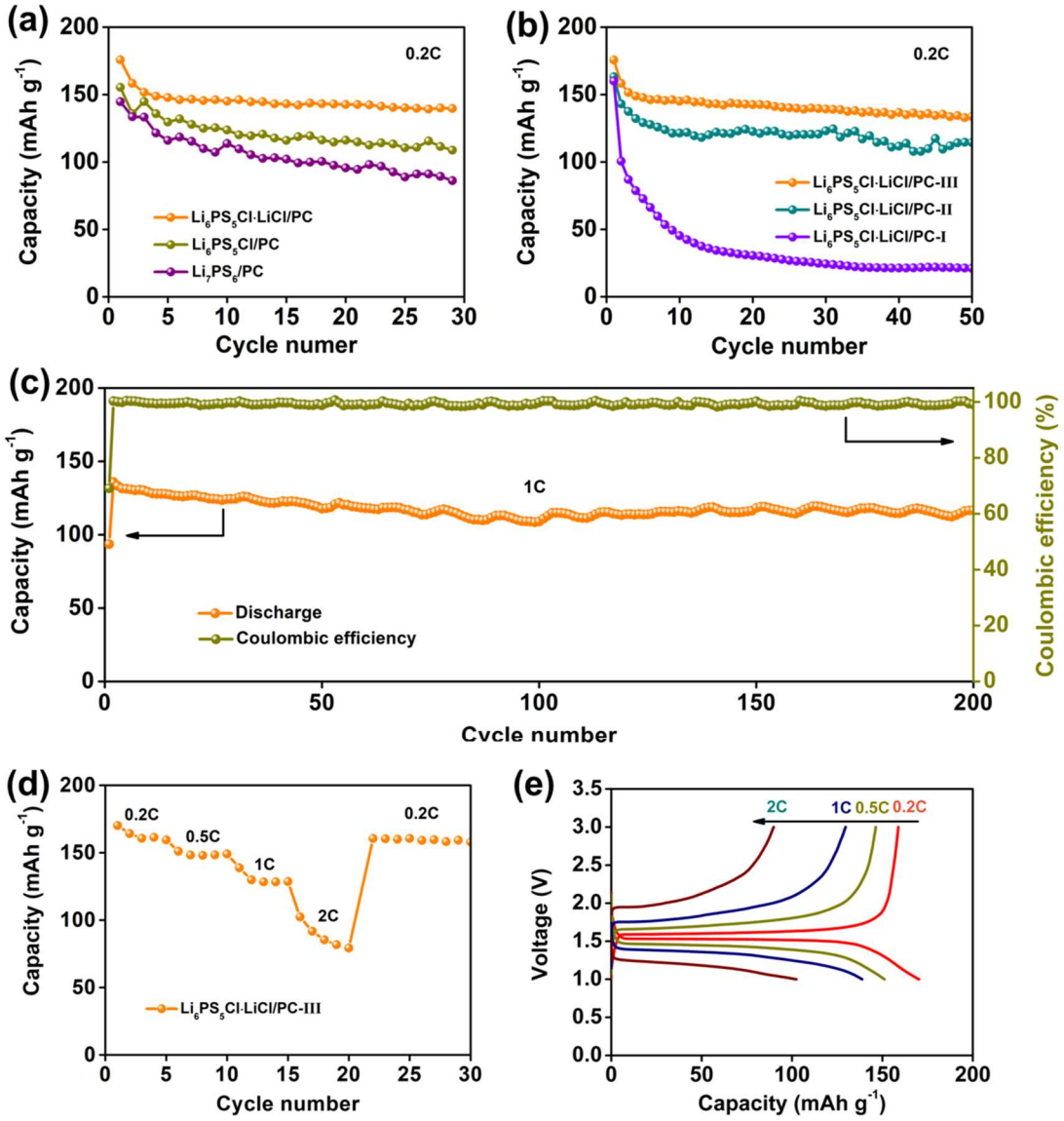

Fig. 4. Cycling performance of (a) the LTO||Li cells with the Li_7PS_6/PC, Li_6PS_5Cl/PC and Li_6PS_5Cl·LiCl/PC at 0.2 C. (b) the LTO||Li cells with the Li_6PS_5Cl·LiCl/PC-I, Li_6PS_5Cl·LiCl/PC-II and Li_6PS_5Cl·LiCl/PC-III at 0.2 C. (c) Cycling performance and Coulombic efficiency of the LTO||Li cell with Li_6PS_5Cl·LiCl/PC at 1 C. (d) Rate capabilities at 0.2 C, 0.5 C, 1 C and 2 C. (e) Charge/discharge curves of the LTO||Li cell with the Li_6PS_5Cl·LiCl/PC at various current rates. (PC-I, II, III refers to different amount of PC, whereas PC-I for 7.9 μL/cm^2, PC-II for 11.8 μL/cm^2, and PC-III for 15.8 μL/cm^2, PC-III was applied for (a)(c)(d)(e)).

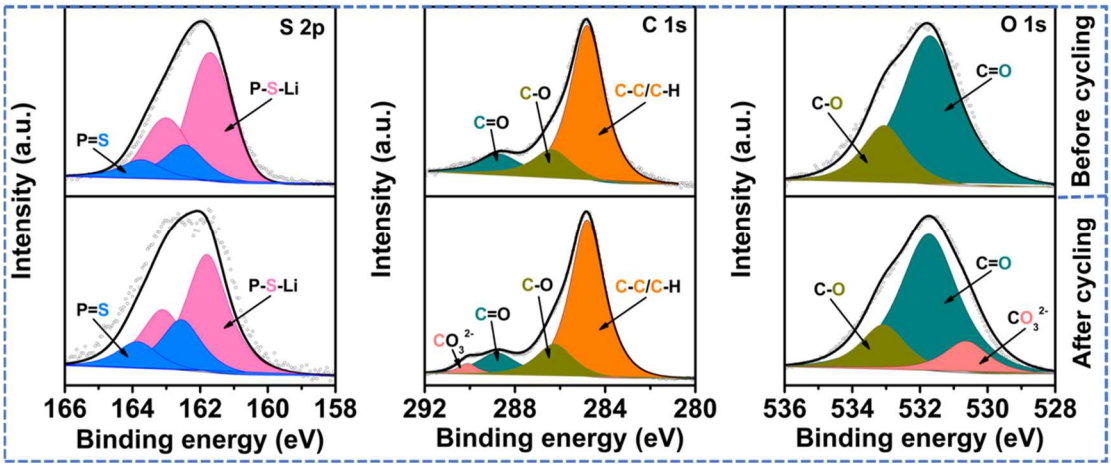

Fig. 5. Detailed XPS spectra and peak fits of S 2p, C 1s and O 1s obtained from SE of the LTO||Li_6PS_5Cl·LiCl/PC|| Li cell before (top) and after cycling (bottom).

Table of Content Graphic